Fluorescence Correlation Spectroscopy Using Octadecylrhodamine B as a Specific Micelle-Binding Fluorescent Tag; Light Scattering and Tapping Mode Atomic Force Microscopy Studies of Amphiphilic Water-Soluble Block Copolymer Micelles†,‡

Jana Humpolíčková and Karel Procházka*

Department of Physical and Macromolecular Chemistry and Laboratory of Specialty Polymers, School of Science, Charles University in Prague, Albertov 6, 128 43 Prague 2, Czech Republic

Martin Hof

The Jaroslav Heyrovský Institute of Physical Chemistry, Academy of Sciences of the Czech Republic and Center for Complex Molecular Systems and Biomolecules, Dolejškova 3, 182 23 Prague 8, Czech Republic

Zdeněk Tuzar and Milena Špírková

Institute of Macromolecular Chemistry, Academy of Sciences of the Czech Republic, Heyrovský Square 2, 162 06 Prague 6, Czech Republic

Received November 25, 2002. In Final Form: February 25, 2003

Amphiphilic multimolecular block copolymer micelles of polystyrene-*block*-poly(methacrylic acid) and polystyrene-*block*-poly(ethylene oxide) were investigated by fluorescence correlation spectroscopy (FCS) in aqueous media using octadecylrhodamine B (ORB) as a micelle-specific probe, together with UV−visible absorption and other fluorescence techniques (steady-state spectroscopy and depolarization and time-resolved fluorescence decay measurements). The aim of the study was to show that the fluorescence techniques alone provide sufficient information on the micellar system, allowing, thus, for the fully conclusive study. Other techniques, such as static and quasi-elastic light scattering and atomic force microscopy were used just for comparison to prove the reliability of the FCS results and estimate their accuracy. The binding kinetics of ORB to micelles in aqueous solutions accompanied by association-dependent changes in UV−vis and fluorescence spectra and the binding equilibrium were also studied because knowledge of them is necessary for the correct interpretation of the FCS results.

Introduction

Fluorescence correlation spectroscopy (FCS) is a relatively new spectroscopic technique that monitors the behavior of fluorescent molecules, fluorescent-tagged macromolecules, and nanoparticles at the molecular level in times ranging from 10^{-6} to 10^{-2} s. This technique was described first by Magde et al. in 1972.[1] In the 1970s and 1980s, its use was limited mostly by the lack of reliable apparatuses. Since the mid-1970s, theoretical principles of FCS and fields of its applications have been developed.[2−14] The most important advances of FCS were reviewed, for example, by Thompson in 1991.[15] With the advent of commercially available apparatuses produced by the company Carl Zeiss, Jena, Germany, the use of FCS spread all over the world in last 10 years. FCS is quite popular among scientists working in biochemical and biomedical fields;[2−4,6,11−14,16−18] nevertheless, it has never found a major use in polymer science. To our knowledge, there were only a few attempts to apply FCS for studying polymeric nanoparticles, and in those studies, FCS was used only as a supplementary technique of the second rank in importance.[19,20] In our opinion, a low

* To whom correspondence should be addressed.

† This study is a part of the Long-Time Research Plan of the Faculty of Science of the Charles University, MSM 1131 00001.

‡ The authors dedicate this paper to Professor Petr Munk, D.Sc., Professor Emeritus at the University of Texas at Austin, TX, on the occasion of his 70th birthday.

(1) Magde, D.; Elson, E. L.; Webb, W. W. *Phys. Rev. Lett.* **1972**, *29*, 705.
(2) Webb, W. W. In *Fluorescence Correlation Spectroscopy Theory and Applications*; Riedler, R., Elson, E. S., Eds.; Springer-Verlag: Berlin, 2001.
(3) Hink, M. A.; van Hoek, A.; Visser, A. J. W. G. *Langmuir* **1999**, *15*, 992.
(4) Koppel, D. E. *Phys. Rev. A* **1974**, *10*, 1938.
(5) Kask, P.; Günter, R.; Axhausen, P. *Eur. Biophys. J.* **1997**, *25*, 163.
(6) Meseth, U.; Wohland, T.; Rigler, R.; Vogel, H. *Biophys. J.* **1999**, *80*, 2987.
(7) Edman, L. *J. Phys. Chem. A* **2000**, *104*, 6165.
(8) Wohland, T.; Rigler, R.; Vogel, H. *Biophys. J.* **2000**, *80*, 2987.
(9) Magde, D.; Elson, E. L.; Webb, W. W. *Biopolymers* **1974**, *13*, 29.
(10) Elson, E. L.; Magde, D. *Biopolymers* **1974**, *13*, 1.
(11) Magde, D.; Webb, W. W.; Elson, E. L. *Biopolymers* **1978**, *17*, 361.
(12) Aragón, S. R.; Pecora, R. *Biopolymers* **1975**, *14*, 119.
(13) Aragón, S. R.; Pecora, R. *J. Chem. Phys.* **1976**, *64*, 1791.
(14) Hess, S. T.; Huang, S.; Heikal, A. A.; Webb, W. W. *Biochemistry* **2002**, *41*, 697.
(15) Thompson, N. L. In *Topics in Fluorescence Spectroscopy*; Lakowicz, J. R., Ed.; Plenum Press: New York, 1991; Vol. 1, Chapter 6.
(16) Beneš, M.; Billy, D.; Hermens, W. T.; Hof, M. *Biol. Chem.* **2002**, *383*, 337.
(17) Král, T.; Hof, M.; Langner, M. *Biol. Chem.* **2002**, *383*, 331.
(18) Beneš, M.; Hudeček, J.; Anzenbacher, P.; Hof, M. *Collect. Czech. Chem. Commun.* **2001**, *66*, 855.
(19) Schuch, H.; Klingler, J.; Rossamanith, P.; Frechen, T.; Gerst, M.; Feldthusen, J.; Müller, A. H. E. *Macromolecules* **2000**, *33*, 1734.

10.1021/la0209334 CCC: $25.00
Published on Web 04/19/2003

interest of polymer scientists in FCS is due to the fact that macromolecules and polymeric nanoparticles strongly scatter visible light and can be studied by light scattering techniques that routinely provide high-precision data of the same type.

The advantages of FCS are the (i) negligible consumption of the sample, (ii) possibility to measure the diffusion coefficients of small molecules that do not scatter light, and (iii) possibility to determine the diffusion coefficients of tagged molecules in mixtures and complex systems that contain excess of nonfluorescent molecules. The method is, however, limited either to fluorescent or fluorescent-tagged particles with extremely low intersystem crossing rates (even fluorescein that is described in relatively new textbooks as a suitable probe[15] undergoes almost total photobleaching at high light intensities used in modern apparatuses).

In this work, we use FCS for investigating block copolymer micelles in aqueous media. Polymeric micelles have been the subject of numerous studies of many research groups because of their interesting potential applications, for example, in the drug and gene delivery systems.[21−24] The number of studies on water-soluble micelles is so vast that it is futile to give all relevant references. Therefore, we mention only a few comprehensive reviews and a representative outline of the most important works.[25−38] We have been studying the micellization of amphiphilic block copolymers, mostly of *block*-polyelectrolytes, in aqueous media by using a combination of fluorescence, light scattering, ultracentrifugation, electrophoresis, and other experimental methods for more than one decade.[39−57] The high-molar-mass amphiphilic copolymers are usually insoluble in water, and the micelles have to be prepared indirectly, for example, by dialysis from aqueous mixtures with organic solvents into purely aqueous media.[39] Multimolecular micelles in water often have kinetically frozen cores. Their water-soluble shell behaves basically as a convex polymeric brush.[58−62] In the case of polyelectrolyte shells formed by annealed (i.e., weak) polyelectrolytes, the solution behavior is strongly influenced by the pH and ionic strength, I, but the dissociation of the ionizable groups in the shell does not correspond to the bulk pH and I.[48,49,60,63,64] The shells of polystyrene-*block*-poly(methacrylic acid) micelles, PS-PMA, studied in this work are formed by weak PMA, which also has some properties of polysoaps.[65−71]

The aims of the paper are the following: (i) We would like to demonstrate that a combination of FCS with steady-state and time-resolved fluorometry, that is, fluorescence techniques, only allow for fully conclusive studies of micelle-based polymeric nanoparticles in aqueous media. Other experimental techniques [quasi-elastic light scattering (QELS), static light scattering (SLS), and atomic force microscopy (AFM)] were employed just to prove that the fluorescence signal alone provides sufficient information on the system. (ii) We present the results of our study of the binding kinetics and equilibrium because this knowledge is necessary for FCS studies on octadecylrhodamine B (ORB)-labeled nanoparticles in aqueous media.

(20) Erhardt, R.; Böcker, A.; Zettl, H.; Kaya, H.; Pychhout-Hintzen, W.; Krausch, G.; Abetz, V.; Müller, A. H. E. *Macromolecules* **2001**, *34*, 1069.

(21) Kwong, G. S.; Naito, M.; Yokoyama, M.; Okano, T.; Sakuray, Y.; Kataoka, K. *Pharm. Res.* **1995**, *12*, 92.

(22) Harada, A.; Kataoka, K. *Macromolecules* **1995**, *28*, 5294.

(23) Kataoka, K.; Harashima, H. *Adv. Drug Delivery Rev.* **2001**, *52*, 151.

(24) Nagasaki, Y.; Yasugi, K.; Yamamoto, Y.; Harada, A.; Kataoka, K. *Biomacromolecules* **2001**, *2*, 1067.

(25) Riess, G.; Hurtres, G.; Bahadur, P. *Encyclopedia of Polymer Science and Engineering*, 2nd ed.; Wiley: New York, 1985; p 234.

(26) Tuzar, Z.; Kratochvíl, P. In *Surface and Colloid Science*; Matijevic, E., Ed.; Plenum Press: New York, 1993; Vol. 15, p 1.

(27) Tuzar, Z. In *Solvents and Self-organization of Polymers*; Webber, S. E., Munk, P., Tuzar, Z., Eds.; NATO ASI Series E; Kluwer Academic Publishers: Dordrecht, 1996; Vol. 327, pp 309, 327.

(28) Wilhelm, M.; Zhao, C.-L.; Wang, Y.; Xu, R.; Winnik, M. A.; Mura, J.-L.; Riess, G.; Croucher, M. D. *Macromolecules* **1991**, *24*, 1033.

(29) Rager, T.; Meyer, W. H.; Wegner, G.; Winnik, M. A. *Macromolecules* **1997**, *30*, 4911.

(30) Astafieva, I.; Khougaz, K.; Eisenberg, A. *Macromolecules* **1995**, *28*, 7127.

(31) Yu, Y. S.; Zhang, L. F.; Eisenberg, A. *Langmuir* **1997**, *13*, 2578.

(32) Shen, H. W.; Zhang, L. F.; Eisenberg, A. *J. Am. Chem. Soc.* **1999**, *121*, 2728.

(33) Shen, H. W.; Eisenberg, A. *J. Phys. Chem. B* **1999**, *103*, 9473.

(34) Antonietti, M.; Heinz, S.; Schmidt, M.; Rosenauer, C. *Macromolecules* **1994**, *27*, 3276.

(35) Regenbrecht, M.; Akari, S.; Förster, S.; Mohwald, H. *J. Phys. Chem. B* **1999**, *103*, 6669.

(36) Buthun, V.; Lowe, A. B.; Billingham, N. C.; Armes, S. P. *J. Am. Chem. Soc.* **1999**, *121*, 4288.

(37) Lee, A. S.; Gast, A. P.; Buthun, V.; Armes, S. P. *Macromolecules* **1999**, *32*, 4302.

(38) Wooley, K. L. *J. Polym. Sci.* **2000**, *38*, 1397.

(39) Tuzar, Z.; Webber, S. E.; Ramireddy, C.; Munk, P. *Polym. Prepr. (Am. Chem. Soc., Div. Polym. Chem.)* **1991**, *32* (1), 525.

(40) Munk, P.; Procházka, K.; Tuzar, Z.; Webber, S. E. *CHEMTECH* **1998**, *28* (10), 20.

(41) Kiserow, D.; Procházka, K.; Ramireddy, C.; Tuzar, Z.; Munk, P.; Webber, S. E. *Macromolecules* **1992**, *25*, 461.

(42) Procházka, K.; Kiserow, D.; Ramireddy, C.; Tuzar, Z.; Munk, P.; Webber, S. E. *Macromolecules* **1992**, *25*, 454.

(43) Ramireddy, C.; Tuzar, Z.; Procházka, K.; Webber, S. E.; Munk, P. *Macromolecules* **1992**, *25*, 2541.

(44) Tian, M.; Quin, A.; Ramireddy, C.; Webber, S. E.; Munk, P.; Tuzar, Z.; Procházka, K. *Langmuir* **1993**, *9*, 1741.

(45) Teng, Y.; Morrison, M.; Munk, P.; Webber, S. E.; Procházka, K. *Macromolecules* **1998**, *31*, 3578.

(46) Štěpánek, M.; Krijtová, K.; Limpouchová, Z.; Procházka, K.; Teng, Y.; Webber, S. E.; Munk, P. *Acta Polym.* **1998**, *49*, 96; **1998**, *49*, 103.

(47) Procházka, K.; Martin, T. J.; Munk, P.; Webber, S. E. *Macromolecules* **1996**, *29*, 6518.

(48) Štěpánek, M.; Procházka, K. *Langmuir* **1999**, *15*, 8800.

(49) Štěpánek, M.; Procházka, K.; Brown, W. *Langmuir* **2000**, *16*, 2502.

(50) Karymov, M. A.; Procházka, K.; Mendenhall, J. M.; Martin, T. J.; Munk, P.; Webber, S. E. *Langmuir* **1996**, *12*, 748.

(51) Štěpánek, M.; Krijtová, K.; Procházka, K.; Teng, Y.; Webber, S. E. *Colloids Surf., A* **1999**, *147*, 79.

(52) Tsisilianis, C.; Voulgaris, D.; Štěpánek, M.; Podhájecká, K.; Procházka, K.; Tuzar, Z.; Brown, W. *Langmuir* **2000**, *16*, 6868.

(53) Procházka, K.; Martin, T. J.; Webber, S. E.; Munk, P. *Macromolecules* **1996**, *29*, 6526.

(54) Štěpánek, M.; Podhájecká, K.; Tesařová, E.; Procházka, K.; Tuzar, Z.; Brown, W. *Langmuir* **2001**, *17*, 4240; **2001**, *17*, 42.

(55) Matějíček, P.; Limpouchová, Z.; Uhlík, F.; Procházka, K.; Tuzar, Z.; Webber, S. E. *Collect. Czech. Chem. Commun.* **2002**, *67*, 531.

(56) Uhlík, F.; Limpouchová, Z.; Matějíček, P.; Procházka, K.; Tuzar, Z.; Webber, S. E. *Macromolecules* **2002,** *35*, 9497.

(57) Matějíček, P.; Uhlík, F.; Limpouchová, Z.; Procházka, K.; Tuzar, Z.; Webber, S. E. *Macromolecules* **2002**, *35*, 9487.

(58) Pincus, P. *Macromolecules* **1991**, *24*, 2912.

(59) Israels, R.; Leermakers, F. A. M.; Fleer, G. J.; Zhulina, E. B. *Macromolecules* **1994**, *27*, 3249.

(60) Lyatskaya, Yu. V.; Leermakers, F. A. M.; Fleer, G. J.; Zhulina, E. B.; Birstein, T. M. *Macromolecules* **1995**, *28*, 3562.

(61) Shusharina, N. P.; Linse, P.; Khokhlov, A. R. *Macromolecules* **2000**, *33*, 3829.

(62) Misra, S.; Mattice, W. L.; Napper, D. H. *Macromolecules* **1994**, *27*, 7090.

(63) Groenewegen, W.; Ugelhaaf, S. U.; Lapp, A.; van der Maarel, J. R. C. *Macromolecules* **2000**, *33*, 3283.

(64) Förster, S.; Hermsdorf, N.; Bottcher, C.; Lindner, P. *Macromolecules* **2002**, *35*, 4096.

(65) Katchalski, A. *J. Polymer. Sci.* **1951**, *7*, 393.

(66) Anufrieva, E. V.; Birshtein, T. M.; Nekrasova, T. N.; Ptitsyn, C. B.; Scheveleva, T. V. *J. Polym. Sci., Part C: Polym. Lett.* **1968**, *16*, 3519.

(67) Koenig, J. L.; Angood, A. C.; Semen, J.; Lando, J. B. *J. Am. Chem. Soc.* **1969**, *91*, 7250.

(68) Ghiggino, K. P.; Tan, K. L. In *Polymer Photophysics*; Phillips, D., Ed.; Chapman and Hall: London, 1985; Chapter 7.

(69) Wang, Y.; Morawetz, H. *Macromolecules* **1986**, *19*, 1925.

(70) Bednář, B.; Trněná, J.; Svoboda, P.; Vajda, Š.; Fidler, V.; Procházka, K. *Macromolecules* **1991**, *24*, 2054.

(71) Soutar, I.; Swanson, L. *Macromolecules* **1994**, *27*, 4304.

Experimental Section

Materials. *ORB.* ORB was purchased from Molecular Probes, U.S.A. (Chart 1).

Solvents. 1,4-Dioxane and methanol were purchased from Aldrich International and used without further purification. Deionized water was used in this study.

Block Copolymer Samples. Diblock copolymer samples of PS-PMA (SA34) were prepared by Dr. C. Ramireddy and Professor P. Munk at the University of Texas at Austin, TX, U.S.A., using anionic polymerization in tetrahydrofuran at −78 °C in a N_2 atmosphere. Their preparation and characterization were described earlier.[41−43] The heteroarm copolymer $PS_{15}PEO_{15}$ with 15 PS and 15 poly(ethylene oxide) (PEO) arms was provided by Professor C. Tsitsilianis from the University of Partas, Greece.[72,73] The molar masses and compositions of the used samples are the following: SA34, $M_w = 4.16 \times 10^4$ g/mol, $M_w/M_n = 1.05$; weight fraction of PS, $x_{PS} = 0.68$; $PS_{15}PEO_{15}$, $M_w = 3.6 \times 10^5$ g/mol, $M_w/M_n = 1.15$; weight fraction of PS, $x_{PS} = 0.14$.

Techniques. *FCS.* All measurements were performed with the binocular microscope Confocor I, Carl Zeiss, Jena, Germany, equipped with a 514-nm argon laser, an adjustable pinhole together with a special fluorescence optics, detection diode SPCM-200PQ, and an ALV-5000 correlator (ALV Langen, Germany). FCS is a technique in which temporal fluctuations in the fluorescence measured from a sample of fluorescent molecules are analyzed to obtain information about processes that give rise to the fluorescence fluctuations. In this work, we focus only on the translational diffusion and photobleaching due to the intersystem crossing as a complicating process. The time-fluctuating fluorescence intensity measured from a small irradiated volume, $F(t)$, is given by the following formula:[15]

$$F(t) = \kappa Q \int W(\mathbf{r}, t)\, C(\mathbf{r}, t)\, d\mathbf{r} \qquad (1)$$

where κ is the proportionality constant; Q is the product of the absorptivity, fluorescence quantum yield, and experimental collection efficiency; $C(\mathbf{r}, t)$ is the concentration of fluorescent species at position $\mathbf{r}$ in time t; and $W(\mathbf{r}, t)$ is a product of the intensity profile of the incident laser beam (usually assumed to be a Gaussian profile) and functions that characterize irradiated volume. The normalized autocorrelation function of fluctuations, which is used for the evaluation of the diffusion coefficients, is given by the following generic equation:

$$G(\tau) = 1 + \langle F(t)\cdot F(t+\tau)\rangle / \langle F(t)\rangle^2 \qquad (2)$$

where $F(t)$ is the fluorescence intensity in time t and $F(t+\tau)$ is the intensity in time $t+\tau$, and the averaging is performed over all measured time intervals. Several models differing in complexity have been treated theoretically.[2−8] According to current experimental conditions, a roughly cylindrical volume of the radius ω_1 and height $2\omega_2$ irradiated by a focused laser beam with a Gaussian intensity profile is usually considered. If this volume contains two types of fluorescent particles with quantum yields ϕ_1 and ϕ_2 and the same probability of the intersystem crossing (e.g., one probe distributed in two different microenvironments), the function $G(\tau)$ assumes the following form:[2,3]

$$G(\tau) = 1 + \frac{1}{N(1-F)}[1 - F(1 - e^{-\tau/\tau_0})] \times \left\{ \frac{1-Y}{1+\tau/\tau_1} \frac{(\phi_1\sigma_1)^2}{[1+S^{-2}(\tau/\tau_1)]^{1/2}} + \frac{Y}{1+\tau/\tau_2} \frac{(\phi_2\sigma_2)^2}{[1+S^{-2}(\tau/\tau_2)]^{1/2}} \right\} \qquad (3)$$

where N is the particle number (i.e., the total number of fluorescent particles in this volume), Y and $(1-Y)$ are molar fractions of both species, ϕ_i is the quantum yield of ith species, σ_i is the absorption cross section, F is the fraction of molecules converted to the triplet state, τ_0 is the average effective lifetime of the triplet state, which reflects the experimental conditions

Chart 1. Structure of ORB

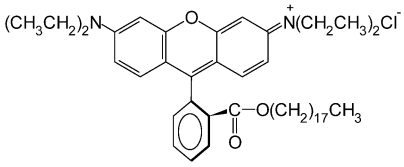

used[74] (i.e., the intensity of the excitation beam, which determines the rate of the excitation to the first singlet state and all transition rates between excited states under given conditions), S is the ratio of half axes, $S = \omega_2/\omega_1$, and the irradiated volume $V = 2\pi\omega_1^2\omega_2$. The diffusion coefficient of the ith component, D_i, may be calculated as $D_i = \omega_1^2/4\tau_i$, and the hydrodynamic radius can be recalculated using the Stokes−Einstein formula, $R_H = kT/6\pi D\eta$, where k is the Boltzmann constant, T is the temperature, and η is the viscosity of the solvent.

Steady-State Fluorometry. Steady-state fluorescence spectra (i.e., corrected excitation and emission spectra and steady-state anisotropy) were recorded with a SPEX Fluorolog 3 fluorometer in a 1-cm quartz cuvette closed with a Teflon stopper. Oxygen was removed by 5 min of bubbling with nitrogen before the measurement.

Time-Resolved Fluorometry. The time-correlated single-photon counting technique was used for measurements of fluorescence lifetimes. The time-resolved fluorescence decays were recorded on a 5000U time-resolved fluorometer (IBH, Great Britain), equipped with an IBH NanoLED-01 (490-nm peak wavelength, 1−1.5-ns full width at half-maximum of the pulse, 1-MHz repetition rate) and cooled microchannel plate−photomultiplier tube (Hamamatsu, Japan). A reconvolution procedure was used to get the true fluorescence decays that were further fitted to multiexponential functions using the Marquardt−Levenberg nonlinear least-squares method using the FLA-900 software (Edinburgh Instruments, Great Britain). Low values of χ^2 (close to 1.0) and the random distribution of residuals were used as criteria of the fit.

SLS. Measurements were performed on a Sofica instrument equipped with a He−Ne laser. Data were treated by the standard Zimm method.[75] Refractive index increments, dn/dc, were measured on a Brice-Phoenix differential refractometer.

Dynamic Light Scattering. An ALV 5000 multibit, multitau autocorrelator (Langen, Germany) and an He−Ne laser ($\lambda = 633$ nm) were employed. The solutions for the measurements were filtered through 0.22-μm Millipore filters. Measurements were performed with solutions of the lowest possible concentration (ca. 0.1 mg/mL) at different angles and a temperature of 25 °C. Analysis of the data was performed by fitting the experimentally measured $g_2(t)$, the normalized intensity autocorrelation function, which is related to the electrical-field correlation function, $g_1(t)$, by the Siegert relation:[49]

$$g_2(t) - 1 = \beta |g_1(t)|^2 \qquad (4)$$

where β is a factor accounting for deviation from the ideal correlation.

The average diffusion coefficient and polydispersity were evaluated using the cumulant method, which employs the relation

$$g_1(t) = \exp[-\Gamma(q)t + \mu_2(q)t^2 + O(t^3)] \qquad (5)$$

The average diffusion coefficient may be obtained from the first term as $D = \Gamma/q^2$ and the polydispersity index of the diffusion-coefficient distribution, P_D, from the second moment of the correlation curve, $P_D = \mu_2(q)/\Gamma(q)^2$. Here, $q = (4\pi n_0/\lambda)\sin(\theta/2)$ is the magnitude of the scattering vector, $\Gamma = 1/\tau$ is the relaxation rate, θ is the scattering angle, n_0 is the refractive index of the pure solvent, and λ is the wavelength of the incident light. The term $O(t^3)$ is a small error on the order of t^3. The hydrodynamic

(72) Voulgaris, D.; Tsitsilianis, C.; Esselink, F. J.; Hadziioannou, G. *Polymer* **1998**, *39*, 6429.

(73) Voulgaris, D.; Tsitsilianis, C.; Grayer, V.; Esselink, F. J.; Hadziioannou, G. *Polymer* **1999**, *40*, 5879.

(74) Widengren, J.; Metz, U.; Rigler, R. *J. Phys. Chem.* **1995**, *99*, 13368.

(75) Kratochvíl, P. In *Classical Light Scattering from Polymer Solutions, Polymer Science Library 5*, Jennkins, A. D., Ed.; Elsevier: Amsterdam, 1987.

radius R_H was evaluated from the diffusion coefficient using the Stokes−Einstein formula.

AFM. All measurements were performed in the tapping mode (TM) under ambient conditions using a commercial scanning probe microscope, Digital Instruments NanoScope dimensions 3, equipped with silicon cantilever Nanosensors with a typical spring constant of 40 N/m. Polymeric micelles were deposited on a fresh (i.e., freshly peeled out) mica surface (flogopite, ideal formula $KMg_3AlSi_3O_{10}(OH)_2$, Geologic Collection of Charles University in Prague, Czech Republic) by a fast dip coating in a dilute micelle solution in pure water (c_P ca. 10^{-3} mg/mL). After the evaporation of water, the samples for AFM were dried in a vacuum oven at an ambient temperature for about 5 h.

Results and Discussion

The spectroscopic behavior of common rhodamine dyes, such as rhodamine B (RB), rhodamine 6G (R6G), and rhodamine 110 in solutions and their behavior at surfaces has been a subject of numerous studies, and at present, their spectra are fairly well-understood.[76−90] The aforementioned dyes are soluble in polar organic solvents and a little soluble in water also, but they have a strong tendency to form dimers and multiple aggregates at higher concentrations (ca. 10^{-3} mol/L for RB).[90] RB forms predominantly H dimers in water and J dimers in lower aliphatic alcohols. Fujii et al., who studied RB in ethanol−water mixtures, were able to decompose the experimental spectra into subspectra of the monomer RB, H dimer RB, and J dimer RB.[90] They reported the monomer absorption maximum at $\lambda_M = 555$ nm (below 10^{-4} M) and the blue- and red-shifted absorption maxima of the H dimer at $(\lambda_B)_H = 525$ nm and $(\lambda_R)_H = 553$ nm and J dimer at $(\lambda_B)_J = 531$ nm and $(\lambda_R)_J = 569$ nm, respectively. We performed similar measurements with RB in methanol−water mixtures, and we found essentially the same values.

The spectroscopic behavior of ORB is similar to that of RB, but it is more influenced by the formation of H and J dimers in aqueous media as a result of the hydrophobically driven association.[91,92] Because the systematic data on the associative and spectroscopic behavior of ORB in mixed aqueous media in a broad range of conditions have not been published so far, we performed a study of ORB in water−methanol solutions before attempting to investigate its binding to polymeric micelles in aqueous media. The new (so far unpublished) data will be published elsewhere. Here, we just point out that the fluorescence of the water-dissolved ORB is strongly self-quenched because this fact is important for the binding studies and interpretation of the FCS data of the ORB-labeled micelles.

Interaction of ORB with Amphiphilic Block Copolymer Micelles. *Preparation of Block Copolymer Micelles and ORB Binding in Aqueous Media.* Polymeric micelles (PS-PMA) were prepared by stepwise dialysis, which is a standard technique for the preparation of aqueous micellar solutions in our laboratory, and characterized by QELS and SLS. The molar mass measured by SLS in aqueous media is $(M_M)_w = 8.0 \times 10^6$ g/mol, and R_H measured by QELS in a low-ionic-strength alkaline borate buffer (pH 9.2, ionic strength $I = 0.015$) is $R_H = 54$ nm.

The amphiphilic ORB dye binds strongly at the core−shell interface of the PS-PMA micelles with its nonpolar aliphatic tail buried in and partially adsorbed to the PS core, similar to the fluorescein- or coumarine-based surfactants.[48,49,51] In the micelle-bound state, the positively charged fluorescent headgroups are located preferentially in a fairly narrow transition region between the dissociated (i.e., ionized) and nondissociated (i.e., neutral) parts of the PMA shell. In the following text, we characterize the amount of ORB molecules in the system by the probe-to-micelle ratio ξ, which gives the average number of probes in the system per one micelle. Because one micelle consists (e.g., for a SA34 sample) approximately of 10^2 molecules, ξ gives the number of ORB molecules per 10^2 PS-PMA chains. It should be kept in mind that, at low ξ, almost all ORB molecules are really sorbed to micelles, whereas at high ξ, a nonnegligible fraction of ORB is dissolved in the bulk aqueous phase (mostly in the form of nonfluorescent aggregates). At fluorophore-to-micelle molar ratios $\xi < 1$, individual fluorophores bind to different micelles and the possibility of dimerization (and higher aggregation) diminishes. For $\xi > 10$, several ORB molecules bind to one micelle, but they are embedded in the inner shell far from each other in the form of individual monomers. Therefore, the emission spectrum changes in favor of the monomer, and the fluorescence quantum yield increases after the binding of ORB to micelles. We have observed the analogous behavior of 5-*N*-octadecanoylaminofluorescein (OAF) and heptadecyl-7-dimethylaminocoumarin in systems of water-soluble polymeric micelles.[51] Figure 1a shows the absorption spectra of ORB at different times after its mixing with the solution of micelles, at the ratio ξ of about 5. It is evident that the dye binds as a monomer because the monomer band increases and the red part (580−610 nm) corresponding to the J aggregates disappears during the binding process. A closer inspection also reveals changes in the region close to 530 nm, which indicate a decrease of the concentration of the H dimers with time. Changes in the shape of the emission spectrum are less pronounced, but the binding is accompanied by a very pronounced increase in the monomer fluorescence intensity. Monitoring the fluorescence intensity around 580 nm is, therefore, the tool of choice for kinetic studies. The inset in Figure 1a shows the corresponding kinetic curve (i.e., fluorescence intensity, I_F, versus time, t). We have tried to decompose the absorption spectra of ORB at the beginning and end of the binding process using the spectra of the J aggregates, H aggregates, and monomer published by Fujii et al.[90] The decomposition is shown in Figure 1b. In the first case, the decomposition requires one more spectrum with the absorption maximum around 570 nm. We assume that the additional spectrum belongs to the higher aggregates of ORB. Immediately after the mixing, the absorption spectrum contains 34% of the monomer spectrum, 18% of the H-dimer spectra, and 48% of the higher aggregate's

(76) Del Monte, F.; Levy, D. *J. Phys. Chem. B* **1998**, *102*, 8036.
(77) Burghardt, T. P.; Lyke, J. E.; Ajtai, K. *Biophys. Chem.* **1996**, *59*, 119.
(78) Vogel, R.; Harvey, M.; Edwards, G.; Meredith, P.; Heckenberg, N.; Trau, M.; Rubinstein-Dunlop, H. *Macromolecules* **2002**, *35*, 2063.
(79) Ray, K.; Nakahara, H. *J. Phys. Chem. B* **2002**, *106*, 92.
(80) Del Monte, F.; Mackenzie, J. D.; Levy, D. *Langmuir* **2000**, *16*, 7377.
(81) Aguirresacona, I. U.; Arbeola, F. L.; Arbeola, I. L. *J. Chem. Educ.* **1989**, *66*, 866.
(82) Chaudhuri, R.; Arbeola, F. L.; Arbeola, I. L. *Langmuir* **2000**, *16*, 1285.
(83) Kemnitz, K.; Yoshihara, K. *J. Phys. Chem.* **1991**, *95*, 6095.
(84) Nakashima, K.; Fujimoto, Y. *Photochem. Photobiol.* **1994**, *60*, 565.
(85) McRae, E. G.; Kasha, M. *Physical Processes in Radiation Biology*; Academic Press: New York, 1964.
(86) Kasha, M.; Rawls, H. R.; El-Bayoumi, A. *Pure Appl. Chem.* **1965**, *11*, 38.
(87) McRae, E. G.; Kasha, M. *J. Chem. Phys.* **1961**, *11*, 38.
(88) Chambers, R. W.; Kajiwara, T.; Kearns, D. R. *J. Phys. Chem.* **1974**, *78*, 380.
(89) Dunsbach, R.; Schmidt, R. *J. Photochem. Photobiol., A* **1995**, *85*, 275.
(90) Fujii, T.; Nishikiori, H.; Tamura, T. *Chem. Phys. Lett.* **1995**, *233*, 424.
(91) Mukerjee, P. *J. Phys. Chem.* **1965**, *69*, 2821.
(92) MacDonald, R. I. *J. Biol. Chem.* **1990**, *265*, 13533.

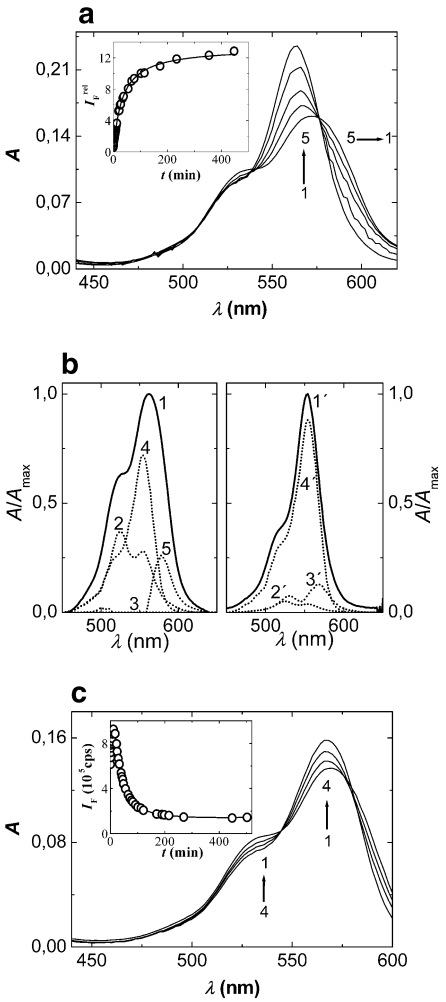

Figure 1. (a) Changes in ORB absorption spectra with time, *t*, upon mixing the ORB with the aqueous solution of PS-PMA micelles for a low ratio of ORB to micelles, ξ of about 5. The experimental conditions were as follows: PS-PMA concentration, $c_P = 7.2 \times 10^{-5}$ mol/L; ORB concentration, $c_F = 3.6 \times 10^{-6}$ mol/L; 0.5 M Borax buffer; time upon mixing, *t* (min) = (curve 1) 0, (curve 2) 11, (curve 3) 37, (curve 4) 135, (curve 5) 547. (Inset) Relative fluorescence intensity at the maximum of the emission band, I_F^{rel}, as a function of time upon mixing, *t*, for ξ of about 5. (b) Decomposition of the absorption spectra of ORB at the beginning and end of the binding process to PS-PMA micelles. Curves 1 and 1′ represent the normalized spectra of ORB immediately upon mixing with the micellar solution and 9 h later, respectively. Curves 2 and 2′, 3 and 3′, and 4 and 4′ are spectra of the H dimer, J dimer, and monomer, respectively. Curve 5 is the spectrum of higher ORB aggregates. The experimental conditions were the same as in Figure 1a. (c) Spectral changes with time upon mixing micelles with ORB for a high ξ of about 500. The experimental conditions were as follows: PS-PMA concentration, $c_P = 7.2 \times 10^{-7}$mol/L; ORB concentration, $c_F = 3.6 \times 10^{-6}$ mol/L; 0.5 M Borax buffer; time upon mixing, *t*(min) = (curve 1) 0, (curve 2) 17, (curve 3) 54, (curve 4) 184. (Inset) Relative fluorescence intensity at the maximum of the emission band, I_F^{rel}, as a function of time upon mixing, *t*, for ξ of about 500.

spectra. At long times, the absorption spectrum can be resolved into 5% of the H-dimer spectra, 12% of the J-dimer spectra, and 83% of the monomer spectra.

We further studied the binding kinetics in the excess ORB, for a ξ of about 250−500. In this case, the shell becomes saturated at long times after mixing the dye with micelles, and the system reaches the partition equilibrium, in which an important fraction of the dye remains dissolved in the aqueous phase. The binding kinetics is fairly fast, and the rate increases with an increasing amount of ORB

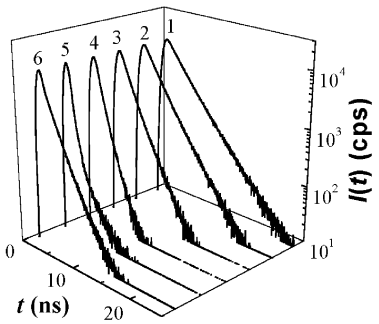

Figure 2. ORF fluorescence decay curves for different ORB-to-micelle ratios ξ. The ORB concentration $c_F = 3.6 \times 10^{-6}$ mol/L. The PS-PMA concentration, c_P, ranges from 6.1×10^{-7} to 1.8×10^{-5} mol/L to yield the following values of ξ: (curve 1) 20, (curve 2) 40, (curve 3) 70, (curve 4) 100, (curve 5) 200, (curve 6) 700. The experimental conditions were as follows: excited by a light-emitting diode at 493 nm, emission monitored at 580 nm.

per micelle. Because a major fraction of ORB remains dissolved in the aqueous phase in all stages of the binding process, the absorption spectra do not change significantly (Figure 1c). The fluorescence intensity increases at early times, but the shell becomes saturated and the emission decreases because of self-quenching due to nonradiative energy transfer to the H dimers (see inset in Figure 1c for ξ ca. 500). These absorption spectra were also decomposed and the results are available upon request.

For a successful FCS study of micellar systems, the knowledge of the partition coefficient K_p^{eff} (at least in orders of magnitude) is necessary because a rough estimate of the fractions of the bound and free probes under the extreme dilutions used in FCS measurements is needed. Because the fluorescence of the water-dissolved ORB is self-quenched, FCS itself does not allow for this estimate. However, it may be obtained by fluorometry if the analysis of the time-resolved data is based on a model that assumes the presence of two types of probes in the system.[48] The first type of probes is (i) the interface-sorbed probes with a fluorescence lifetime $\tau_{F_1} = 2.8$ ns in the absence of H dimers. This value compares quite well with the lifetimes measured by Fayer et al. for ORB bound to SDS or Triton surfactant micelles.[93,94] (ii) The probes dissolved in the bulk solvent with a fluorescence lifetime $\tau_{F_2} = 1.3$ ns represent the second type of probes. The mean experimental value is shorter than the lifetimes observed in aliphatic alcohols,[95] which is obviously due to the self-quenching of the ORB fluorescence in water (it should be mentioned that the decay is not strictly single-exponential). Molar fractions of probes of the first type, F_1, and second type, F_2, vary with ξ and may be evaluated experimentally from a series of decay curves with increasing ξ (see Figure 2). The effect of the nonradiative energy transfer and quenching of fluorescence from the micelle-bound probes increases with increasing ξ, and a new contribution (basically proportional to $t^{1/a}$, where *a* is a constant; $a > 1$) appears in the fluorescence decay functions. We assume that the fluorescence quenching is due to the Förster excitation-energy transfer from the probes to the traps that are randomly distributed in a relatively large three-dimensional domain (as compared with the Förster radius). Therefore, we use a value of

(93) Quitevis, E. L.; Marcus, A. H.; Fayer, M. D. *J. Phys. Chem.* **1993**, *97*, 5762.
(94) Ediger, M. D.; Dominique, R. P.; Fayer, M. D. *J. Chem. Phys.* **1984**, *80*, 1246.
(95) Visser, A. J. W. G.; Vos, K.; van Hoek, A.; Santema, J. S. *J. Phys. Chem.* **1988**, *92*, 759.

$a = 2$, which allows for reasonably precise fits. Earlier, we have found that the simple fitting formulas (provided, e.g., by Edinburgh Instruments software), which do not take into account the finite size of micelles nor a possible nonrandomness in the distribution of fluorophores, yield sound estimates.[48] The time-resolved emission intensities, $I_F(t)$, may be fitted to the following theoretical curve:[96]

$$I_F(t) = \alpha_1 \exp\left(-\frac{t}{\tau_{F_1}} - 2\gamma\sqrt{\frac{t}{\tau_{F_1}}}\right) + \alpha_2 \exp\left(-\frac{t}{\tau_{F_2}}\right) \quad (6)$$

where the pre-exponential factors α_i are proportional to the molar fractions of the probes and reflect the fact that the short-living probes contribute to the emission intensity at early times more than the long-living probes and, therefore, $F_1 = \alpha_1\tau_F(\gamma)/[\alpha_1\tau_F(\gamma) + \alpha_2\tau_{F_2}]$. The ratio $\tau_F(\gamma)/\tau_{F_1}$ corresponds to the ratio of the steady-state emission intensities from the donor (i) in the presence of the traps, and (ii) in the absence of the traps, $\tau_F(\gamma)/\tau_{F_1} = I_{DT}/I_D$ and can be evaluated from time-resolved data on the basis of the following formula:

$$\tau_F(\gamma) = \tau_{F_1}\int_0^\infty \exp(-s - 2\gamma\sqrt{s})\, ds = \tau_{F_1}[1 - \sqrt{\pi\gamma}\, \exp(\gamma^2)\,(1 - \mathrm{erf}\,\gamma)] \quad (7)$$

where γ is a constant characterizing the contribution of the excitation-energy transfer. It depends on the actual trap concentration, $\gamma = c_T/c_T^0$, where c_T^0 is the critical concentration of the traps for which the rate of energy transfer from the donors to the traps equals the rate of the radiative deactivation of the excited state by fluorescence. Analysis of the time-resolved data, which is described in detail in our earlier paper,[48] yields the value of K_p of about 1.5×10^5. The obtained value is very similar to that for 5-*N*-dodecanoylaminofluorescein (DAF) in the same micellar system. It is necessary to keep in mind that the evaluation accuracy is lower than that in the case of, for example, DAF;[48] nevertheless, it gives a sound estimate of the partition coefficient, sufficient for a correct interpretation of FCS data. The factors decreasing the accuracy are the following: (i) the nonquenched fluorescence decay is not strictly singe-exponential and (ii) the analysis may be applied only in the region of low ξ to avoid the formation of fluorescent J dimers, which are not included in the model.

Studies of PS-PMA and PS-PEO Micelles by FCS. The purpose of the study was to develop and test the FCS research methodology for the characterization of polymeric micelles. As mentioned above, the FCS finds a number of applications in biochemistry,[2−4,6,11−14,16−18] but it was very seldom used in studies of polymeric micelles.[19,20]

The obtained fluorometric data show that ORB is a suitable dye for FCS studies of amphiphilic polymeric micelles in aqueous media for several reasons. The estimate of the partition coefficient is sufficiently high, K_p of about 10^5, showing that the fraction of free ORB is lower than 10% under common FCS conditions. Furthermore, the fluorescence from the free (water-dissolved) probes is self-quenched and does not significantly contribute to the monitored fluctuations. The quantum yield of the micelle-bound ORB is high, and the singlet−triplet intersystem transition rate is low. The fraction of molecules in the triplet state depends on the laser intensity.[74] The triplet lifetime is influenced by the presence of oxygen. In our measurements, the triplet fraction of RB in water was less than 10% and that of ORB in methanol was around 15%, and the triplet lifetimes of RB and ORB were estimated (under conditions used for the study of micelles, i.e., in the presence of oxygen) as being around 12 μs in both cases. The aforementioned findings are very important because the experimental correlation curve can be treated as that describing a single-diffusion mode only, affected by the transition to the triplet state only slightly. When fitting the FCS autocorrelation curve, quite a large number of parameters have to be evaluated. A possibility of choosing a fluorophore with suitable properties to minimize the number of parameters to be fitted considerably increases the reliability of the study and the accuracy of the results.

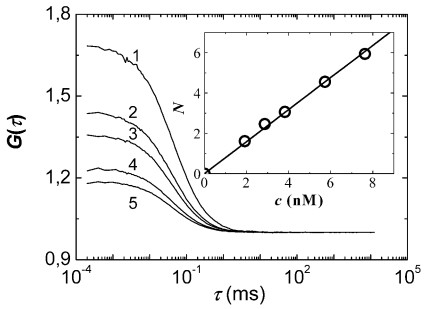

Figure 3. Autocorrelation curves of methanolic solutions of ORB with increasing concentrations (excited by an argon laser at 514 nm, monitored at λ higher than 580 nm). ORB concentration c_F (nmol/L) = (curve 1) 1.91, (curve 2) 2.86, (curve 3) 3.81, (curve 4) 5.72, (curve 5) 7.63. (Inset) Particle number N as a function of ORB concentration.

Before studying polymeric micelles, we characterized the diffusive properties of the ORB monomer in methanol and, also, indirectly in water. In Figure 3, several autocorrelation curves for different concentrations of the probe are shown. A linear dependence of the particle number N (number of fluorescing particles in the focused volume) on the concentration of ORB is shown in the inset. The fitted autocorrelation functions yield the diffusion coefficient of ORB in methanol, $D_M = (5.1 \pm 0.3) \times 10^{-10}$ m^2/s. Using the literature values for the viscosities of methanol and water, we get the diffusion coefficient in water $D_W = (3.0 \pm 0.2) \times 10^{-10}$ m^2/s. The obtained values compare fairly well with the literature diffusion coefficient of R6G in water (i.e., $D_{R6G} = 2.8 \times 10^{-10}$ m^2/s). Because RB and ORB are relatively large molecules, their diffusion coefficients are several times smaller than those of low-molar-mass molecules in nonviscous solvents (e.g., $D_{phenol} = 0.89 \times 10^{-9}$ m^2/s and $D_{toluene} = 0.85 \times 10^{-9}$ m^2/s in water at 20 °C).[97]

At first, we determined the molar mass of the PS-PMA micelles (SA34) in water directly from the particle number N, measured as a function of the increasing ORB-to-micelle ratio ξ. The advantage of this method is that we do not need parameters from the fit of the autocorrelation curve. This approach is reasonably accurate even if the measurement does not provide the high-quality autocorrelation curve. The principle of the determination is the following: In the region of low ξ (<1) values, individual ORB molecules bind to different micelles and the fluorescence emission from the micelle-bound ORB is not self-quenched. The fraction of tagged micelles increases with increasing ξ, and the particle number N rises until each micelle is tagged by at least one ORB molecule. For higher values of ξ, the fluctuations caused by the appearance (or

(96) Eisenthal, K. B.; Siegel, S. *J. Chem. Phys.* **1964**, *41*, 652.

(97) *CRC Handbook of Chemistry and Physics*, 76th ed.; Lide, R. D., Ed.; CRC Press: Boca Raton, FL, 1995; pp 6−257.

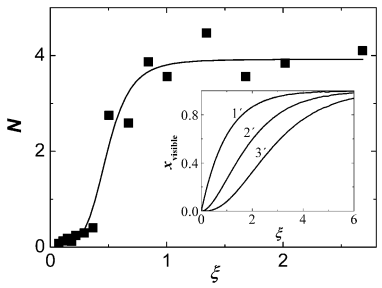

Figure 4. Experimental plot of N versus ξ for the determination of the molar mass of the PS-PMA micelles. The experimental conditions were as follows: PS-PMA concentration, $c_P = 7.65 \times 10^{-7}$ mol/L; ORB concentration, c_F ranges from 5.6×10^{-10} to 2.1×10^{-8} mol/L; 0.05 M Borax buffer. (Inset; curve 1′) Effect of the Poisson distribution of the probes among micelles on the N-versus-ξ plot and simultaneous effect of the Poisson distribution of the probes among micelles together with the impurity quenching on the N-versus-ξ plot, (curve 2′) medium quenching—only the double-tagged micelles are registered, and (curve 3′) strong quenching—only the triple-tagged micelles are registered.

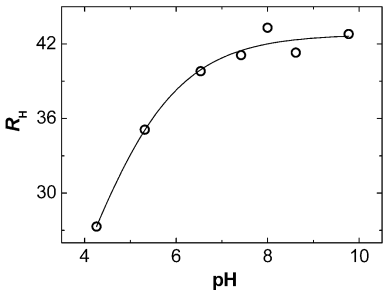

Figure 5. pH-dependent changes in the R_H of the PS-PMA micelles. Concentration of the PS-PMA copolymer $c_P = 1.4 \times 10^{-6}$ mol/L; concentration of ORB $c_{ORB} = 2.8 \times 10^{-7}$ mol/L.

disappearance) of double-tagged micelles from the active volume are more intense than those corresponding to single-tagged micelles but they affect neither the time-dependent autocorrelation function of fluctuations nor the particle number. If we assume the Poisson distribution of the probes among micelles,[98] the N-versus-ξ dependence should theoretically follow curve 1′ in the inset in Figure 4. A similar procedure was also used by other authors for the determination of the association numbers in systems of surfactant micelles, although the possibility of impurity quenching was not taken into account (see further discussion).[99] The experimental dependence of the particle number N on the probe-to-micelle ratio ξ is shown in Figure 4 for the PS-PMA micelles in a Borax buffer. It is obvious that the experimental curve differs significantly from the theoretical curve. It has a sigmoidal shape and is almost equal to 0 in the region of very low ξ values.

The difference between the observed and theoretical curves is obviously due to impurity quenching. In previous sections, we have shown that ORB fluorescence increases after binding to micelles, for low ξ. The steady-state and time-resolved fluorescence measurements are performed for higher ORB and micelle concentrations and for fairly low, but still significantly higher, ORB-to-micelle ratios, than those used in the FCS study. The water-soluble polymeric micelles are known to solubilize various hydrophobic and amphiphilic compounds. Therefore, a low fraction of hydrophobic impurities (which remain in the sample after the polymerization) concentrate in micelles during dialysis and quench the fluorescence. The quenching is important at low values of ξ and changes the shape of the N-versus-ξ dependence. Nevertheless, it does not affect the measurement of M_n. Theoretical curves based on the model that assumes the Poisson distribution of ORB among micelles and different levels of the impurity quenching are shown in the inset of Figure 4. If we assume that we monitor only the double-tagged micelles, the N-versus-ξ dependence corresponds to curve 2′. If the detector "sees" only the triple-tagged micelles, the measurement yields curve 3′. It is evident that in systems where the fluorescence quenching cannot be a priori ruled out, the micellar molar masses can always be evaluated correctly from the leveling-off part of the curve for large values of ξ.

For the PS-PMA concentration in the region of 10^{-7} mol/L and the probe concentration ranging from 10^{-10} to 10^{-8} mol/L, we obtain the micellar molar mass $(M_M)_n = (4.7 \pm 1.1) \times 10^6$ g/mol. The accuracy of the measurement depends strongly on the determination of the effective irradiated volume. The value $V = (8.8 \pm 1.8) \times 10^{-19}$ m^3, was obtained by a careful calibration using the R6G standard (with a known diffusion coefficient). We obtained a higher value for M_w of about 8.0×10^6 g/mol by SLS for SA34 micelles in aqueous media (for identical copolymers and the same preparation technique) in our previous studies.[54] Nevertheless, it is necessary to keep in mind that the value obtained by FCS represents a number-average molar mass, M_n, while that measured by light scattering is the weight-average molar mass, M_w. It will be shown in the next section that a small, however, nonnegligible, polydispersity revealed by AFM can account for differences between M_n and M_w.

For the second example of the M_n determination, we studied a heteroarm copolymer, $PS_{15}PEO_{15}$, in aqueous media. The experimental values in aqueous media, that is, $M_n = 4.1 \times 10^5$ g/mol (measured by FCS) and $M_w = 4.6 \times 10^5$ g/mol (measured by SLS), are quite similar and correspond roughly to the unimer, $M_w = 3.6 \times 10^5$ g/mol, which is a reasonable observation. Because the copolymer structure with collapsed PS and expanded PEO blocks is reminiscent of that of the multimolecular micelle, the sample forms unimer micelles in aqueous media if the dialysis is used. Recently, we have observed a similar behavior for the heteroarm copolymer with a high number of soluble poly(2-vinylpyridine) arms, $PS_{20}PVP_{20}$.[52] It is worth mentioning that the direct dissolution of the sample leads to irreproducible low aggregates, depending on the conditions used (temperature, stirring, etc.). A low polydispersity (manifested by a fairly small difference between the FCS and the SLS results) corresponds roughly to that of the unimer.

Finally, we measured the R_H of the fluorescent-tagged PS-PMA micelles under different conditions. The hydrodynamic radius of micelles formed by copolymers with annealed (i.e., weak) polyelectrolyte blocks depends strongly on the pH and ionic strength because these factors affect the ionization and, consequently, the stretching of the shell-forming blocks.[49,50] We measured the hydrodynamic radii of the PS-PMA micelles as a function of the pH in buffers with a constant ionic strength I (Robinson–Britton buffer, $I = 0.15$). The results are shown in Figure 5. The curve is similar to the one that we obtained for analogous micellar systems in our earlier studies using QELS.[49] In buffers with a relatively high ionic strength,

(98) We assume that the distribution of the probes sorbed to micelles obeys the Poisson distribution, $P(n) = \langle n \rangle^n \exp(-\langle n \rangle)/n!$, which means that, for example, for an average number of probes $\langle n \rangle = 1$ (one probe per micelle) we have $P(n) = (1/e)(1/n!)$; that is, the fraction of probes $P(0) = 0.35$ contains no probes, $P(1) = 0.35$ contains one probe, and the rest are the double- and triple-tagged micelles, etc.

(99) Bastiaens, P. I. H.; Pap, E. H. W.; Widengren, I.; Riegler, R.; Visser, A. J. W. G. *J. Fluoresc.* **1994**, *4*, 337.

$I = 0.15$, the electrostatic repulsion between the COO^- groups is partially screened out but the increase in R_H with pH is obvious.

In regard to the hydrodynamic radius, its evaluation is based on the diffusion coefficient of the micelle-bound ORB. The hydrodynamic radius is calculated using the Stokes−Einstein formula (similar to QELS evaluation). With FCS, we study the diffusion of the tightly micelle-bound probes, that is, the translation diffusion of micelles only. Some authors studied the behavior of the probes bound to surfactant micelles, and using the time-resolved fluorescence anisotropy, they were able to resolve a fairly fast wobbling-in-cone motion from the lateral diffusion of the probe in micelles within the lifetime of the probe on the scale of nanoseconds.[93,100] The FCS study does not allow for this type of measurement. The probes enter into or disappear from the active volume as a result of the translation diffusion either as free probes (essentially invisible because their fluorescence is, in this study, self-quenched) or as the micelle-bound probes. Their motion within the irradiated volume (i.e., fast but spatially limited motion in a slowly moving micelle) does not lead to the monitored fluctuations.

Because the shell of the PS-PMA micelle is very dense compared with the interfacial layer in surfactant micelles, we assume that ORB is firmly bound to micelles with its fluorescent headgroup immersed and almost immobilized in a fairly dense part of the shell. We did not measure the time-resolved fluorescence anisotropy of the micelle-bound ORB, but our recent steady-state measurements with similar micellar systems labeled by OAF and DAF yielded very high values of steady-state fluorescence anisotropy $\langle r \rangle$, ranging from 0.16 at a high pH to 0.3 at a low pH (i.e., according to the expansion the PMA shell).[49]

TMAFM Study. To get more detailed information on the size distribution of micelles and understand the differences between the FCS and the SLS results, we investigated micellar systems by AFM. We performed the TMAFM studies on micelles deposited on a fresh hydrophilic mica surface by a dip coating technique. The AFM samples were prepared from dilute solutions of micelles in the range of 10^{-1}−10^{-3} mg/mL. The size and shape of surface-adsorbed micelles differ from those in the solution (micelles are deformed and resemble "pancakes", but we are interested mainly in the relative size distribution to account for the differences between the number- and the weight-average molar masses. It is generally recognized that the highly hydrophilic mica surface is negatively charged, and, therefore, it has been widely used for binding polycations.[101−104] Our PS-PMA micelles are highly charged polyanions; nevertheless, they stick well to the fresh mica surface. Mica (flogopite) is composed of two-dimensional layers of covalent aluminumsilicate polyanion networks. The layers are kept together by electrostatic forces with small cations (mainly alkaline, K^+, and alkaline earth, Mg^{2+}) inserted between the layers. The freshly peeled-off mica surface is covered by cations, and its net charge is roughly neutral. The surface cations may be washed out, but our time-dependent pH measurements with mica particles dispersed in water show that within the first few seconds, only a negligible fraction of cations is released into the aqueous phase. We use a fast dip coating (ca. 1 s) to get the reproducible deposition of micelles at the surface.

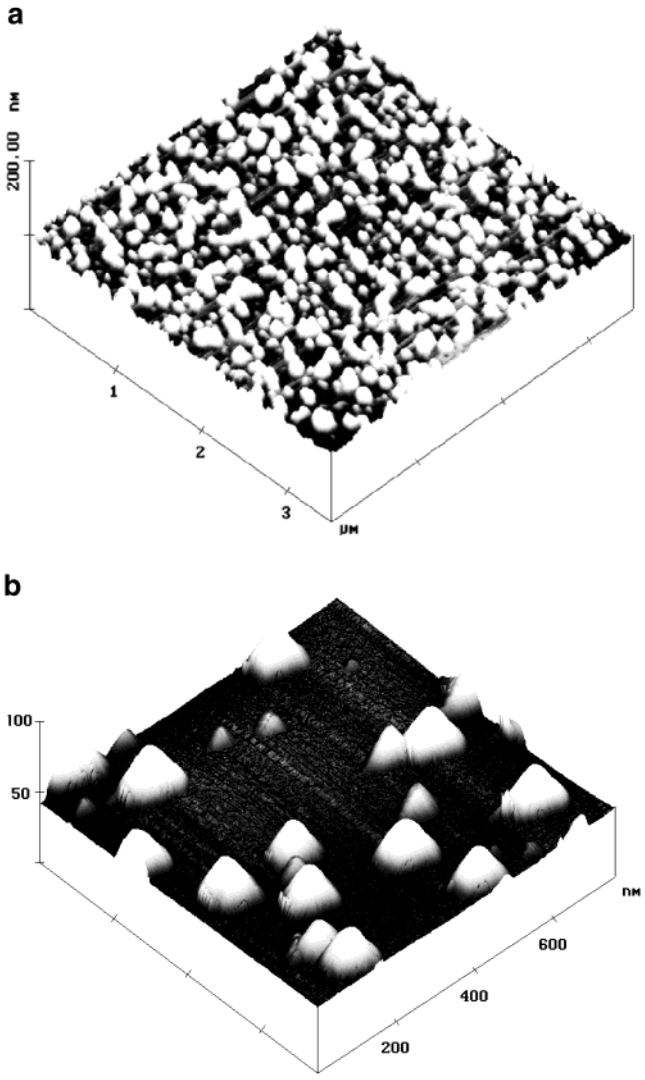

Figure 6. (a) Tilted 3.5 × 3.5 μm tapping mode AFM scan of a mica surface highly covered by PS-PMA micelles. The high surface coverage was obtained by a fast dip coating in an aqueous solution of micelles; copolymer concentration c_P is about 1.0×10^{-1} mg/mL. (b) A tilted 800 × 800 nm tapping mode AFM scan of PS-PMA micelles deposited on a mica surface by a fast dip coating from a dilute aqueous solution of micelles (copolymer concentration c_P ca. 5.0×10^{-3} mg/mL). A typical example of the vertical profiles of the surface-deposited micelles is shown below the scan.

Figure 6a shows the surface-deposited micelles from a relatively concentrated solution (c_P ca. 10^{-1} mg/mL). A tilted three-dimensional TMAFM 3.5 × 3.5 × 100 nm scan (scan rate ca. 0.1 Hz) shows a fairly dense deposition of micelles on the fresh mica surface. At this concentration, the micelles are deposited next to each other and some of them are overlaid. This is why we see micelles with an admixture of micellar clusters. A nonnegligible polydispersity in the micellar sizes and presence of a nonnegligible fraction of smaller micelles are well-apparent. This AFM scan demonstrates a strong tendency of the negatively charged PS-PMA micelles to adsorb on the fresh mica surface. To suppress a possible cluster formation at the surface, the solution was diluted about 16 times by pure water, and a new 800 × 800 × 50 nm scan (scan rate ca. 0.3 Hz) was performed (Figure 6b). It is evident that the formation of micellar clusters was prevented. Hence, we

(100) Sen, S.; Sukul, D.; Dutta, P.; Bhattacharyya, K. *J. Phys. Chem. A* **2001**, *105*, 7495.
(101) Hartley, P. G.; Scales, P. J. *Langmuir* **1998**, *14*, 6948.
(102) Zhmund, B. V.; Meurk, A.; Bergstrom, L. *J. Colloid Interface Sci.* **1998**, *207*, 332.
(103) Claesson, P. M.; Ninham, B. W. *Langmuir* **1992**, *8*, 1406.
(104) Briscoe, W. H.; Horn, R. G. *Langmuir* **2002**, *18*, 3945.

may conclude that the clusters do not form in the solution. The average vertical difference (obtained form the cross-sectional analysis, which is not shown) is around 20 nm, which compares well with the diameter of the core. The average horizontal diameter of the micelles is about 100 nm. This value corresponds to micelles with their shell-forming blocks spread on the surface. As mentioned above, we are interested mainly in the size distribution, which should reflect that in the solution. The AFM scan shows clearly the presence of a low fraction of smaller micelles, which are "hardly visible" for QELS and SLS, but they contribute to the value measured by FCS, thus lowering the number-average molar mass, M_n. This finding accounts for the difference between the values of the molar masses of micelles measured by either SLS or FCS.

Conclusions

1. The study shows that ORB is a suitable probe for FCS studies on micellar systems for several reasons: (i) Similar to its parent compound, RB, the monomer ORB has a high fluorescence quantum yield and a low transition rate to the triplet state. (ii) The spectroscopic behavior of ORB in aqueous media (which was studied, but the data will be published elsewhere) is complex. The probe is not very soluble in water and forms aggregates that self-quench the fluorescence from the water-dissolved dyes, which is convenient for the FCS studies of polymeric micelles. (iii) It shows very high binding affinity to micelles, and the fraction of the free probe in aqueous micellar solutions is low under conditions used in FCS experiments. (iv) At low probe-to-micelle ratios, ORB binds as individual monomers, and its fluorescence quantum yield increases upon binding. With respect to the above-mentioned facts, the FCS detector "sees" only the diffusion of the fluorescent-tagged micelles because the fluorescence from a low concentration of free fluorophores is self-quenched. Hence, the autocorrelation curve of fluorescence fluctuations may be interpreted as that caused by the single-component diffusion only. It is also very important that the autocorrelation curve is only little affected by the transition to the triplet state. Therefore, the use of ORB as a micelle-specific probe results in the minimization of the number of parameters that have to be fitted, which increases the accuracy and reliability of the study.

2. FCS was used to study PS-PMA and PS-PEO micelles in water. The molar masses and hydrodynamic radii measured by FCS were compared with those obtained by the highly recognized "benchmark" techniques, such as SLS and QELS. The molar mass measurement, which is based only on the number of fluorescent particles in the irradiated volume and does not require fitting the autocorrelation curve, yields reliable and accurate data. The FCS values are smaller compared with those of SLS as a result of the fact that the former technique yields the number-average molar masses, M_n, whereas the latter provides the weight-average molar masses, M_w. The comparison of hydrodynamic radii of micelles measured by FCS and QELS suggests that the QELS accuracy is probably better for highly scattering nanoparticles; nevertheless, FCS provides reasonable data.

3. The AFM study performed on PS-PMA micelles deposited on a mica surface shows that the micelles, which appear fairly monodispersed according to QELS, exhibit some polydispersity. They contain a low, albeit non-negligible, fraction of significantly smaller particles, which accounts for the lower micellar masses obtained by FCS in comparison with those obtained by light scattering techniques.

Acknowledgment. This study was supported by the Grant Agency of the Czech Republic (K.P. and Z.T., Grant 203/01/0536; M.Š., Grant 203/01/0735) and the Grant Agency of the Charles University (Grant 215/2000/BCh/Pr). M.H. and J.H. would also like to acknowledge the support of the Ministry of Education of the Czech Republic (LN 00A032). The authors are indebted to Professor P. Munk from the University of Texas at Austin, TX, U.S.A., and Professor C. Tsitsilianis from the University of Patras, Greece, for block copolymer samples.

LA0209334